ISSN 1062-8738, Bulletin of the Russian Academy of Sciences: Physics, 2010, Vol. 74, No. 12, pp. 1715–1717. © Allerton Press, Inc., 2010.
Original Russian Text © A.G. Rzhanov, S.E. Grigas, 2010, published in Izvestiya Rossiiskoi Akademii Nauk. Seriya Fizicheskaya, 2010, Vol. 74, No. 12, pp. 1785–1788.

Dynamical Model of Silicon Evanescent Laser[1]

A. G. Rzhanov and S. E. Grigas
Moscow State University
e-mail: rjanov@mail.ru

Abstract—Numerical self-consisted dynamical model of silicon evanescent laser is developed. *P–I* characteristics and mode composition of laser radiation are obtained. Dynamical processes are investigated, self-modulation mode is observed.

DOI: 10.3103/S106287381012021X

INTRODUCTION

Over the past few years silicon photonics has experienced tremendous growth [1–4]. The main reason is the possibility to fabricate devices compatible with *CMOS* technology which is widely used in microelectronics. Using silicon as the main building material allows fabrication of low-cost optoelectronic devices. In the past few years significant progress has been made in fabrication of passive silicon based devices such as modulators [5], photodetectors [6], and interconnects [7], but still it is difficult to achieve lasing in silicon. The problem is the extremely low probability of radiative recombination because of silicon indirect band structure. Different approaches to fabricate silicon laser have been demonstrated including nanocrystalline silicon structures [8], Si/Ge quantum cascade structures [9–11], Raman lasers [12]. The most successful approach is the hybrid integration of III–V quantum well heterostructure with silicon waveguide [13–17]. This type of laser is called hybrid silicon evanescent laser (*SEL*). A lot of experimental data can be found in the literature concerning *SEL's* but still there is a need of theoretical research in this area. Numerical self-consistent dynamical model of electrically pumped hybrid silicon evanescent laser is presented in this paper.

DYNAMICAL MODEL

Cross section of electrically pumped *SEL* is schematically shown at Fig. 1 [14]. The laser consists of two regions: silicon-on-insulator (*SOI*) passive rib waveguide and classical laser heterostructure that provides optical gain. *SOI* waveguide width w is of 2.5 μm, height h is of 0.69 μm and rib etch depth d is of 0.52 μm. Active region is based on AlGaInAs quantum wells with photoluminescence peak at 1303 nm. The laser is electrically pumped through the contacts shown at Fig. 1. Optical radiation propagates mainly through the silicon waveguide and laser gain in such structure is achieved due to silicon waveguide optical mode overlapping with an active layer.

We have developed numerical self-consistent dynamical model of the *SEL* based on the next assumptions:

—quasi-stationary approximation;

—uniform distribution of light intensity and carrier concentration in z–y plane (coordinate system is shown at Fig. 1);

—carrier diffusion is neglected.

Carrier concentration and photon density dynamics in the resonator are described by coupled rate equations (for example see [18]). On the assumptions mentioned above these equations take on form

$$\frac{dN(t)}{dt} = \frac{J}{ed} - \frac{N(t)}{\tau_{sp}} - \sum_{i=1}^{m} \tilde{\Gamma}_i G_i(t) S_i(t), \tag{1}$$

$$\frac{dS_1(t)}{dt} = \tilde{\Gamma}_1 \Gamma G_1(t) S_1(t) - \frac{S_1(t)}{\tau_p} + \Gamma\beta \frac{N(t)}{\tau_{sp}}, \tag{2}$$

$$\frac{dS_m(t)}{dt} = \tilde{\Gamma}_m \Gamma G_m(t) S_m(t) - \frac{S_m(t)}{\tau_p} + \Gamma\beta \frac{N(t)}{\tau_{sp}}, \tag{3}$$

where $S_i(t)$—resonator volume-averaged i-th optical mode photon density, $N(t)$—active layer volume-

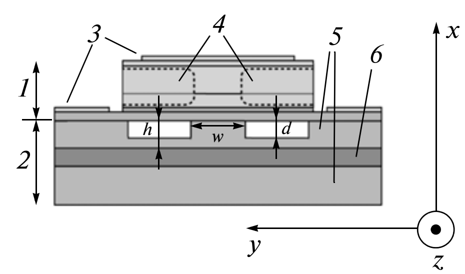

Fig. 1. Silicon evanescent laser schematic [14]: *1*—laser heterostructure; *2*—*SOI* silicon waveguide; *3*—electrical contacts; *4*—proton implanted regions; *5*—silicon; *6*—silicon dioxide.

[1] The article was translated by the authors.

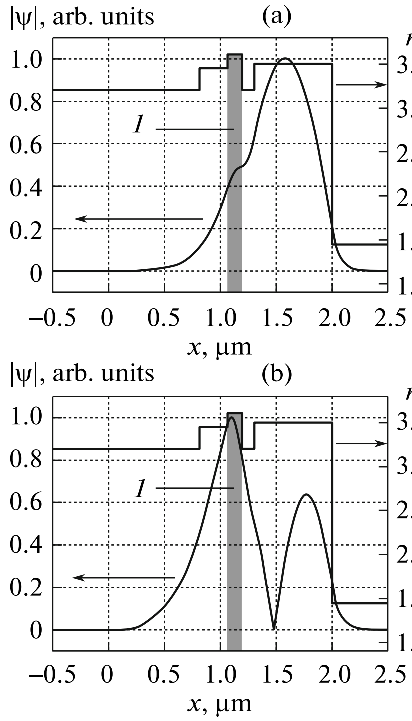

Fig. 2. Hybrid laser structure optical mode profiles: (a) TE_0, (b) TE_1. $|\psi|$ —magnitude of normalized non-zero electrical field component; n—profile of the real part of refractive index; *1*—active region, x—spatial coordinate x.

averaged carrier concentration, J—pump current density, e—electron charge, d—active layer thickness, τ_{sp}—carrier spontaneous recombination time, τ_p—photon lifetime in the resonator, β—spontaneous recombination coefficient (fraction of spontaneous radiation that is amplified), $G_i(t)$— i-th mode optical gain, Γ and $\tilde{\Gamma}_i$—optical confinement factors, m—number of transversal optical modes which are taken into account.

First equation states that the speed of carriers concentration variations depends on spontaneous and stimulated recombination rate and electrical pumping. Second and subsequent equations state that photon density variation speed depends on photon production rate, spontaneous recombination rate and photon losses in the resonator.

Intensity evolution of i-th optical mode can be described in terms of gain coefficients $G_i(t)$, which can be calculated as:

$$G_i(t) = -2\,\mathrm{Im}\,\omega_i(t), \tag{4}$$

where Im represents imaginary part of a complex number.

These gain coefficients are time-dependent because i-th optical mode complex frequency ω_i (complex eigen-value of scalar wave equation) varies with time. To obtain G_i resonant frequencies ω_i are calculated at the first stage from the resonator parameters for a given wavelength by solving scalar wave equation. Then gain coefficients are used to calculate carriers concentration at the next time step from Eqs. (1–4). Carrier concentration variations lead to active layer refractive index variations, so it is necessary to recalculate resonant frequencies at which laser generation occurs and optical modes gain coefficients at every time step in finite-difference algorithm. Total computational time directly depends on the time required for resonant frequency calculation. To decrease this time and enhance computational efficiency of the algorithm we used special computational technique that was proposed earlier in [19].

Two lower order optical mode profiles calculated at the beginning of simulation are shown at Fig. 2. Spatial intensity distribution was calculated at every time step during the simulation with resonator optical properties variations taken into account. Confinement factor defined as the ratio of the average value of electromagnetic field intensity in the active region to its average value in the resonator was calculated for each optical mode:

$$\tilde{\Gamma}_i = \frac{\int\limits_{V_{\mathrm{act}}} |\psi_i(x)|^2 dV / V_{\mathrm{act}}}{\int\limits_{V_{\mathrm{cav}}} |\psi_i(x)|^2 dV / V_{\mathrm{cav}}},$$

where $\psi_i(x)$—i-th optical mode profile, V_{act}—active region volume and V_{cav} —cavity volume.

RESULTS

Proposed algorithm was used to determine laser structure mode composition. As it follows from Fig. 2 first-order mode overlapping with an active region is considerably higher than that one for the fundamental mode. Therefore laser generation is expected only for the first-order mode. This result is confirmed by experimental data [14]. Thus spatial separation between active region and silicon waveguide leads to laser single-mode operation.

The developed model allows us to calculate *SEL's* power characteristics. Output radiation intensity as a function of time for a given pump current value was calculated. After the transient processes have finished output radiation power can be evaluated. Implementation of this procedure to several pump current values allows us to obtain laser *P–I* characteristic. This characteristics and corresponding experimental data [14] are shown at Fig. 3. Approximations for linear sections of *P–I* characteristics are also presented. Calculated values of threshold current and curve slope—31 mA and 0.57 W/A correspondingly—are in good agreement with experimental data: threshold pump current of 29 mA and linear section slope of 0.42 W/A.

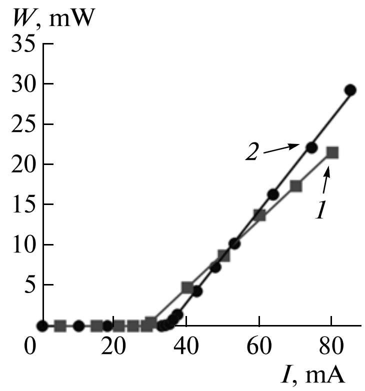

Fig. 3. *SEL's* output power W as a function of drive current I. *1*—Experimental data [14]; *2* —obtained numerical results. Approximations for linear sections of P–I characteristics take the following form: $W = 0.5706\,I — 19.798$ for numerical results, $W = 0.4243\,I — 12.228$ for experimental data.

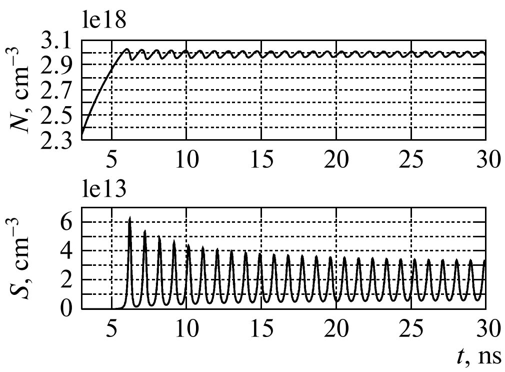

Fig. 4. Self-modulation in *SEL* at 1.22 times the threshold pump current. N—carrier concentration in active region, S—photon density in the resonator.

Dynamical properties of *SEL* were also investigated. It was shown that laser current-step response is the typical inversion population and photon density relaxation oscillation process.

Relaxation oscillations can be described in the following way. Carrier concentration in the active layer gradually increases after the pump current is turned on. Optical mode begin to lase, the carrier concentration having reached threshold value for this mode. Photon density of this mode in the resonator considerably increases while the inverted population decreases. When carrier concentration decreases beyond the threshold value gain coefficient becomes negative and the concerned mode stops to lase. Then carrier concentration reaches threshold value due to pump current again an the process repeats itself. Thus after the pump current step photon density and carrier concentration begin to oscillate until they reach stationary values.

When the pump current reaches some critical value laser response takes the form of periodical self-sustained pulses. An example of such self-modulation process at 1.22 times the threshold pump current is shown at Fig. 4. The oscillation frequency is about 1 GHz. Self-modulation in *SEL's* is of great interest since it provides higher signal-to-noise ratio in optical communication and optical storage read-write systems.

CONCLUSIONS

Self-consisted dynamical model of silicon evanescent laser has been developed. *SEL's* output power as a function of drive current and its mode composition have been obtained. These results are in good agreement with published experimental data. Dynamical processes in *SEL* have been investigated, possibility of automodulation operation mode has been demonstrated.

REFERENCES

1. Jalali, B., et al., *IEEE Microwave Mag.,* 2006, vol. 7, p. 58.
2. Tsybeskov, L., et al., *Proc. IEEE,* 2009, vol. 97, no. 7, p. 1161.
3. Soref, R.A., *Proc. IEEE,* 1993, vol. 81, p. 1687.
4. Bisi, O., Campisano, S.U., Pavesi, L., and Priolo, F., *Silicon Based Microphotonics: from Basics to Applications*, Amsterdam: IOS Press, 1999, p. 279.
5. Marris-Morini, D., et al., *Proc. IEEE*, 2009, vol. 97, no. 7, p. 1199.
6. Vivien, L., et al., *Opt. Express*, 2009, vol. 17, no. 8, p. 6252.
7. Sure, A., *Opt. Express*, 2003, vol. 11, p. 3555.
8. Canham, L.T., *Appl. Phys. Lett.,* 1990, vol. 57, p. 1046.
9. Soref, R.A., *Thin Solid Films*, 1997, vol. 294, p. 325.
10. Dehlinger, G., et al., *Science*, 2000, vol. 290, p. 2277.
11. Diehl, L., *Appl. Phys. Lett.*, 2002, vol. 84, p. 4700.
12. Boyraz, O. and Jalali, B., *Opt. Express,* 2004, vol. 12, no. 21, p. 5269.
13. Park, H., et al., *Opt. Express*, 2005, vol. 13, no. 23, p. 9460.
14. Chang, H.H., et al., *Opt. Express,* 2007, vol. 15, no. 18, p. 11466.
15. Koch, B.R., et al., *Opt. Express*, 2007, vol. 15, no. 18, p. 11225.
16. Fang, A.W., et al., *Opt. Express*, 2008, vol. 16, no. 7, p. 4413.
17. Fang, A.W., et al., *J. Sel. Top. Quant. Electron.,* 2009, vol. 15, no. 3, p. 535.
18. Mroziewicz, B., Bugajski, M., and Nakwaski, W., *Physics of Semiconductor Lasers*, Warszawa: PWN, 1991.
19. Rzhanov, A.G. and Grigas, S.E., *Vychisl. Metody Program.*, 2009, vol. 10, no. 2, p. 72.